Acta Cybernetica **27** (2026) 313–336.

Online Interval Depth Localization of an Underwater Robot with Ballast

Luc Jaulin[ab]

Abstract

This paper presents an efficient online method to simulate a dynamical system with interval uncertainties. These uncertainties can be either on the initial state vector, on the time-dependent inputs, or on the evolution function. Compared to other techniques used for the guaranteed integration of differential inclusion, the presented approach is online and requires a small and fixed number of operations at each sampling time. An illustration related to underwater robotics will be provided. The application involves a robot with a ballast that can move from the surface to the sea floor. We would like to guarantee that the robot will reach a given depth at a given time.

Keywords: differential inclusion, ballast, underwater robot, interval analysis, interval integration, reachability

1 Introduction

Reachability has been studied by many authors using set-membership tools [4, 6, 9, 10, 11, 21, 27]. Often, the objective of reachability is to predict the future of a dynamical system under uncertainties [26]. In this paper, we will focus on an underwater robot equipped with a ballast, namely a *float*, shown in Figure 1.

The float can only move upward to the surface and downward to the seafloor. The state equations are given by

$$\left\{\begin{array}{rcl} \dot{s} &=& u \\ \dot{v} &=& \frac{g\beta s}{1+\beta s} - \frac{c_x}{2(1+\beta s)\ell}\, v\cdot|v| \\ \dot{d} &=& v \end{array}\right. \tag{1}$$

where the state variables are:

[a]Robex, Lab-STICC, ENSTA-Bretagne, France
[b]E-mail: lucjaulin@gmail.com, ORCID: 0000-0002-0938-0615

DOI: 10.14232/actacyb.314709

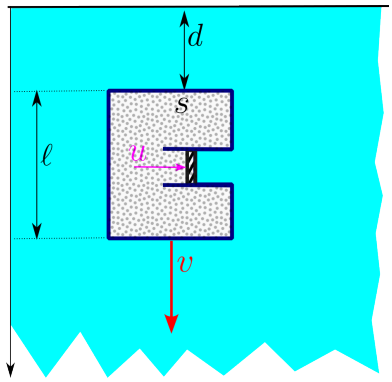


Figure 1: The buoyancy of the robot may change depending of the position of the piston

- The sinking coefficient s (or buoyancy) which corresponds to the position of the piston of the ballast. When $s = 0$, the density of the float is exactly that of the water ρ_0. When $s > 0$, the float sinks and when $s < 0$, it surfaces. The derivative of s can be controlled by a motor and corresponds to the input u. Equivalently, u corresponds to rate of fluid which enters in the ballast.
- The depth d expressed in meters. It is the derivative of the vertical speed.
- The vertical speed v. Its evolution depends of the forces (gravitational, buoyant, drag).

The parameters, assumed to be constant, are:

- The acceleration due to gravity g
- The amplification rate of the piston β: When the piston of the ballast is at position s, the average density of the robot is $(1 + \beta s)$.
- The drag coefficient c_x with respect to the vertical.
- The length ℓ with respect to the vertical position

To get this model, it suffices to apply the Newton's second Law:

$$m\dot{v} = \underbrace{mg}_{\text{gravitational force}} - \underbrace{\rho_0 A\ell g}_{\text{buoyant force}} - \underbrace{\frac{1}{2}c_x\rho_0 A \cdot v \cdot |v|}_{\text{drag force}} \tag{2}$$

where ρ_0 is the density of the water, and A is the cross-sectional area of the robot. Since the mass of the float is $m = (1 + \beta s)\,\rho_0 A\ell$, we get

$$\dot{v} = g - \frac{\rho_0 A\ell g}{(1 + \beta b)\,\rho_0 A\ell} - \frac{1}{2}\frac{c_x\rho_0 A v \cdot |v|}{(1 + \beta b)\,\rho_0 A\ell} \tag{3}$$

which corresponds to (1). Note that much more accurate models can be found in [18].

We assume that we know intervals containing the initial state variables and a tube (*i.e.*, an interval of trajectories) containing the input $u(t)$. Our goal is to find a tube for the three state variables. The notion of tube is illustrated by Figure 2. A tube can be seen as an array containing two lists of intervals: the *gates* $[x](k)$ and the *slices* $[\![x]\!](k)$ (see [24]). A tube is the set of all trajectories that cross all gates and that are always enclosed in the slices. More formally, the slices and the gates are intervals that should satisfy

$$\begin{array}{ll} \forall k, x(k\delta) \in [x](k) & \text{(for the gates)} \\ \forall t \in [(k-1)\delta, k\delta], x(t) \in [\![x]\!](k) & \text{(for the slices)} \end{array} \tag{4}$$

For simplicity, this tube is denoted by $[x](t)$.

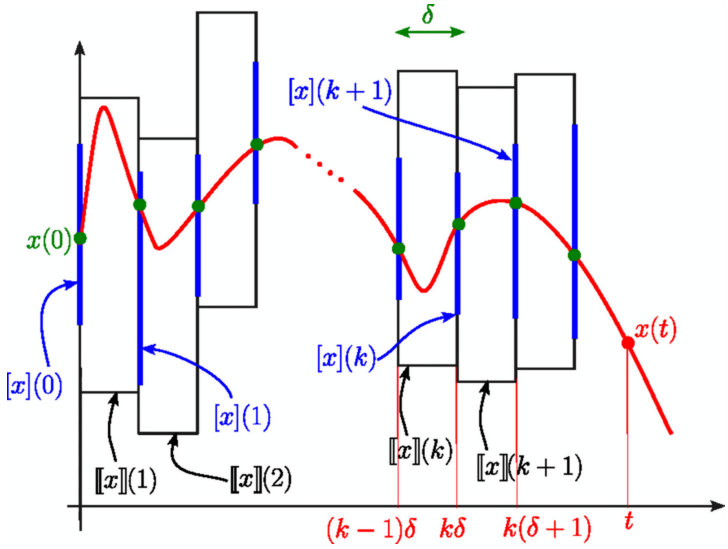


Figure 2: A tube which encloses the trajectory $x(t)$

We can now be more precise on the problem we want to solve. Assume that

- we know an initial box $[s_0^-, s_0^+] \times [v_0^-, v_0^+] \times [d_0^-, d_0^+]$ containing the state (s, v, d) at time $t = 0$.
- we know a tube $[u](t)$ containing $u(t)$ for all $t \geq 0$.

We want to find a tube for each state variable. Moreover, we want the method to be online [22]. More precisely, as illustrated by Figure 3, we want an interval

estimator of the form

$$\begin{pmatrix} [s](k) \\ [v](k) \\ [d](k) \end{pmatrix} = \mathcal{F}\left(\begin{pmatrix} [s](k-1) \\ [v](k-1) \\ [d](k-1) \end{pmatrix}, [\![u]\!](k)\right)$$
$$\begin{pmatrix} [\![s]\!](k) \\ [\![v]\!](k) \\ [\![d]\!](k) \end{pmatrix} = \mathcal{G}\left(\begin{pmatrix} [s](k-1) \\ [v](k-1) \\ [d](k-1) \end{pmatrix}, [\![u]\!](k)\right) \quad (5)$$

such that the corresponding tubes enclose the signals $s(t), v(t), d(t)$. Note that we have gates $[s](k), [v](k), [d](k)$ for s, v, d and a slice $[\![u]\!](k)$ for u. The interval state estimator should execute a fixed set of operations at each sampling time, otherwise we do not have an online predictor. As a consequence, interval methods based on Picard fixed point methods ([2, 13, 20]), bisection based methods (see, e.g., [14]) are not allowed. Moreover, the memory used by estimator should be fixed and thus zonotope approaches [1, 3, 7] should be avoided. In our case, only the three gates for s, v, d will be memorized.

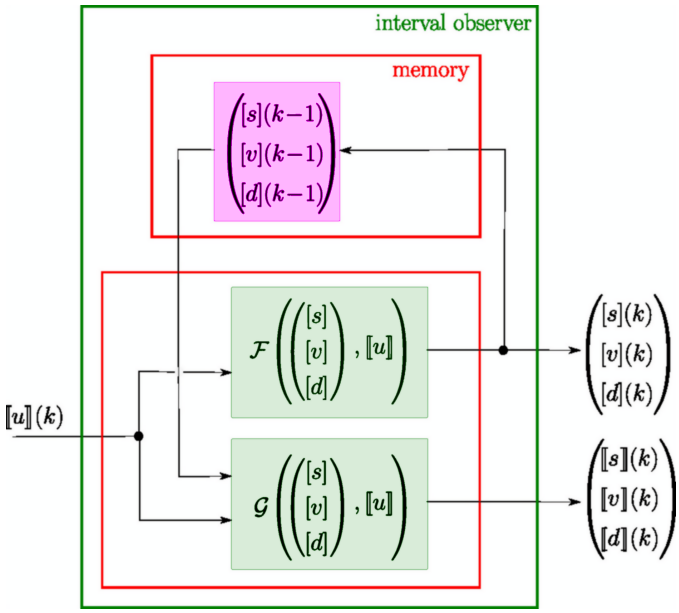


Figure 3: Online interval state estimator

We will take advantage of the fact that the float is composed of three SISO (Single-Input Single-Output) systems in series, as illustrated by Figure 4.

The paper is organized as follows. Section 2 recalls some classical results for differential inclusion for systems with a single state variable. Section 3 introduces the notion of *interval flow* which will be main operator used for a reliable discretisa-

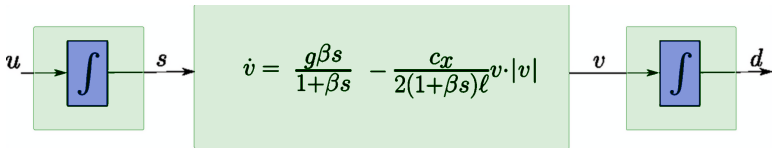


Figure 4: The float is composed of three SISO systems in series

tion of differential inclusions. Section 4 studies the well-known Riccati differential equation. This part will be needed for the resolution of the sinking body problem proposed in Section 5. Section 6 combines all these tools to derive an online interval predictor for the float with interval uncertainties. Section 7 concludes the paper.

2 Differential inclusion

This section recalls some classical results related to differential inclusions [5]. These results will be used further in order to build a reliable procedure to predict the evolution of the float with interval uncertainties.

We consider the scalar system

$$\begin{array}{c} \dot{v}(t) = f(v(t), \mathbf{u}(t)) \\ v(0) = v_0 \in [v_0] \\ \mathbf{u}(t) \in [\![\mathbf{u}]\!] \subset \mathbb{R}^n \end{array} \tag{6}$$

The signal $\mathbf{u}(t)$ is inside the box $[\![\mathbf{u}]\!] \subset \mathbb{R}^m$. Note that $\mathbf{u}(t)$ in chosen as a vector and this is why is it written bold. It varies with time in contrast to the box $[\![\mathbf{u}]\!]$ which is assumed to be constant with time. We have here a differential inclusion [5] with many solutions, as many as we have different signals $\mathbf{u}(t)$ in the box $[\![\mathbf{u}]\!]$. Finding an envelope for the set of all solutions $v(t)$ is a difficult problem which can be solved using optimal control theory [15] for some cases.

2.1 Comparison theorem

We recall here a theorem which can be used directly to find an envelope for a differential inclusion with one state variable [8]. It takes into account the monotonicity of the subsystems [25] to facilitate the interval integration.

Proposition. *Assume that the initial condition satisfies* $v_0 \in [v_0^-, v_0^+]$ *and denote by* $[f]$ *an inclusion function for* f *[17]. An envelope for any solution* $v(t)$ *is* $[v^-(t), v^+(t)]$*, where:*

$$\begin{array}{rcl} \dot{v}^- & = & lb([f](v^-, [\mathbf{u}])) \quad , \quad v^-(0) = v_0^- \\ \dot{v}^+ & = & ub([f](v^+, [\mathbf{u}])) \quad , \quad v^+(0) = v_0^+ \end{array} \tag{7}$$

The operator lb takes the lower bound of its interval input and ub returns its upper bound.

Proof. The minimal and maximal solutions for (6) satisfy [16]:

$$\begin{array}{rcll} \dot{v} & = & f(v, \underset{\mathbf{u}\in[\mathbf{u}]}{\text{argmin}} f(v,\mathbf{u})) & , \quad v(0) = v_0^- \\ \dot{v} & = & f(v, \underset{\mathbf{u}\in[\mathbf{u}]}{\text{argmax}} f(v,\mathbf{u})) & , \quad v(0) = v_0^+ \end{array} \tag{8}$$

It is a consequence of the *Hamilton-Jacobi-Bellman* theorem in the scalar case [15]. Let us recall the comparison theorem for scalar differential equations

$$\left.\begin{array}{c} \dot{x}_1 = \varphi_1(x_1) \\ \dot{x}_2 = \varphi_2(x_2) \\ \varphi_1 \leq \varphi_2 \\ x_1(0) \leq x_2(0) \end{array}\right\} \Rightarrow \forall t, x_1(t) \leq x_2(t). \tag{9}$$

Now, for all v, we have

$$\begin{array}{rcl} \text{lb}([f](v^-,[\mathbf{u}])) & \leq & f(v^-, \underset{\mathbf{u}\in[\mathbf{u}]}{\text{argmin}} f(v^-,\mathbf{u})) \\ \text{ub}([f](v^+,[\mathbf{u}])) & \geq & f(v^+, \underset{\mathbf{u}\in[\mathbf{u}]}{\text{argmax}} f(v^+,\mathbf{u})) \end{array} \tag{10}$$

Therefore, using the comparison theorem, we conclude the proof of the proposition. □

2.2 Example: the sinking body

We consider a body totally immersed in the ocean as represented by Figure 5. As it will be seen later this example is chosen since it is an important component of our underwater robot.

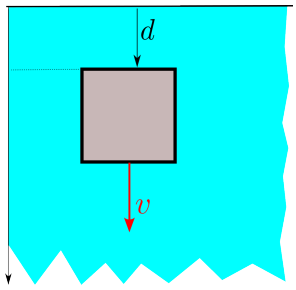


Figure 5: Sinking body

The speed v of the body satisfies the following differential equation

$$\dot{v} = a - bv|v| \tag{11}$$

where $b > 0$ corresponds to a dumping coefficient. If the body has a negative buoyancy, the coefficient a is positive and the body sinks toward the bottom. If it

has a positive buoyancy, a is negative and the body goes up toward the surface. We assume that both a and b are constant and belong to the intervals $[a^-, a^+]$, and $[b^-, b^+]$, respectively.

First, note that the system is stable and $v(t)$ converges to

$$\bar{v} = \text{sign}(a)\sqrt{\frac{|a|}{b}}. \tag{12}$$

Taking into account Proposition 2.1, we get a tube $[v^-, v^+]$ containing $v(t)$. The two bounds v^- and v^+ are defined by the two differential equations

$$\begin{array}{rcl} \dot{v}^- & = & \underbrace{\text{lb}\left([a] - [b]v^-|v^-|\right)}_{f^-_{[a],[b]}(v^-)} \quad , \quad v^-(0) = v_0^- \\ \dot{v}^+ & = & \underbrace{\text{ub}\left([a] - [b]v^+|v^+|\right)}_{f^+_{[a],[b]}(v^+)} \quad , \quad v^+(0) = v_0^+ \end{array} \tag{13}$$

The tube $[v^-, v^+]$ is minimal, *i.e.*, it is the smallest with respect to the inclusion which contains all feasible $v(t)$. As a consequence, we can find a good approximation for the two bounds $v^-(t)$ and $v^+(t)$ using any Runge-Kutta method. For example:

$$\begin{array}{rcl} v^-(t+\delta) & = & v^-(t) + \delta \cdot f^-_{[a],[b]}\left(v^-(t) + \frac{\delta}{2} \cdot f^-_{[a],[b]}(v^-(t))\right) \\ v^+(t+\delta) & = & v^+(t) + \delta \cdot f^+_{[a],[b]}\left(v^+(t) + \frac{\delta}{2} \cdot f^+_{[a],[b]}(v^+(t))\right) \end{array} \tag{14}$$

If δ is small, this approximation is very close to the minimal tube, but it does not provide any guarantee. Guaranteed bounds will be given later in Section 5.

We consider four illustrative cases, illustrated by Figure 6.

Case a We have $(v_0, a, b) \in [0.9, 1.1] \times [0.9, 1.1] \times [1.9, 2.1]$. This means that for $t = 0$, the body goes to the bottom. Since $a > 0$, it sinks (as represented by stones in the cube of the subfigure at the top). The two trajectories $v^-(t)$,$v^+(t)$ in red are obtained by the Runge-Kutta integration (14). We observe that the velocity interval $[v^-(t), v^+(t)]$ converges to the interval $[\bar{v}] = \text{sign}\,([a])\sqrt{\frac{|[a]|}{[b]}}$.

Case b We have $(v_0, a, b) \in [-1.1, -0.9] \times [-1.1, -0.9] \times [1.9, 2.1]$. This means that for $t = 0$, the body goes to the surface. Since $a < 0$, it floats (as represented by the bubbles in the cube of the Subfigure (b)). Again, the two trajectories $v^-(t)$,$v^+(t)$ in red are obtained by the Runge-Kutta integration (14). And again, we observe that $v(t)$ converges to a value $\bar{v}$.

Case c We have $(v_0, a, b) \in [0.9, 1.1] \times [-1.1, -0.9] \times [1.9, 2.1]$. For $t = 0$, the body is thrown toward the bottom. Since $a < 0$, the body floats. We observe that after approximately 1 sec, the body stops sinking and then starts its course to the surface. For the simulation, we need to compute the time at which $v(t)$ changes its sign.

Case d We have $(v_0, a, b) \in [-1.1, -0.9] \times [0.9, 1.1] \times [1.9, 2.1]$. For $t = 0$, the body is thrown toward the surface. Since $a > 0$, the body sinks. We observe that after approximately 1 sec, the body stops surfacing and then starts its course to the bottom.

3 Interval flow

In the previous section, we have shown how an integration of a differential inclusion can be performed in case of interval uncertainties. However, no guarantee was provided, mainly with respect to the time discretisation. In order to get a reliable integration approach, this section presents the new notion of interval flow.

3.1 Interval flow

Given a sampling time $\delta > 0$, an *interval flow* associated with (6) is a function Φ_f which satisfies

$$\Phi_f : \begin{array}{ccc} \mathbb{R} \times \mathbb{IR} \times \mathbb{IR}^m & \to & \mathbb{IR} \times \mathbb{IR} \\ (\delta, [v_0], [\![\mathbf{u}]\!]) & \to & ([v], [\![v]\!]) \end{array} \tag{15}$$

with

$$\left.\begin{array}{c} v(0) \in [v_0] \\ \forall t \in [0, \delta], \mathbf{u}(t) \in [\![\mathbf{u}]\!] \\ \dot{v}(t) = f(v(t), \mathbf{u}(t)) \\ ([v], [\![v]\!]) = \Phi_f(\delta, [v_0], [\![\mathbf{u}]\!]) \end{array}\right\} \Rightarrow \left\{\begin{array}{c} v(\delta) \in [v] \\ \forall t \in [0, \delta], v(t) \in [\![v]\!] \end{array}\right. \tag{16}$$

The interval flow will be used for the discretisation of a differential inclusion. Indeed, if we know an interval for the state $v(t_k)$ at time $t_k = k\delta$, and if we know an interval for the input $u(t)$ for all $t \in [t_k, t_k + \delta]$ the interval flow returns an interval containing $v(t)$, $t \in [t_k, t_k + \delta]$ and an interval for $v(t_k + \delta)$.

3.2 Example: the integrator

Consider the integrator with an uncertain input $u(t)$ and initial state v_0:

$$\left\{\begin{array}{c} \dot{v}(t) = u(t) \\ v(0) = v_0 \in [v_0] \\ u(t) \in [\![u]\!] = [u^-, u^+] \end{array}\right. \tag{17}$$

From Proposition 2.1, we know that any solution $v(t)$ is inside $[v^-(t), v^+(t)]$, where:

$$\begin{array}{rclcl} \dot{v}^- & = & u^- & , & v^-(0) = v_0^- \\ \dot{v}^+ & = & u^+ & , & v^+(0) = v_0^+ \end{array} \tag{18}$$

As a consequence, an interval flow is

$$\Phi_f(\delta, [v_0], [\![\mathbf{u}]\!]) = \left(\begin{array}{c} [v_0] + \delta [\![u]\!] \\ [v_0] + [0, \delta] \cdot [\![u]\!] \end{array} \right) \tag{19}$$

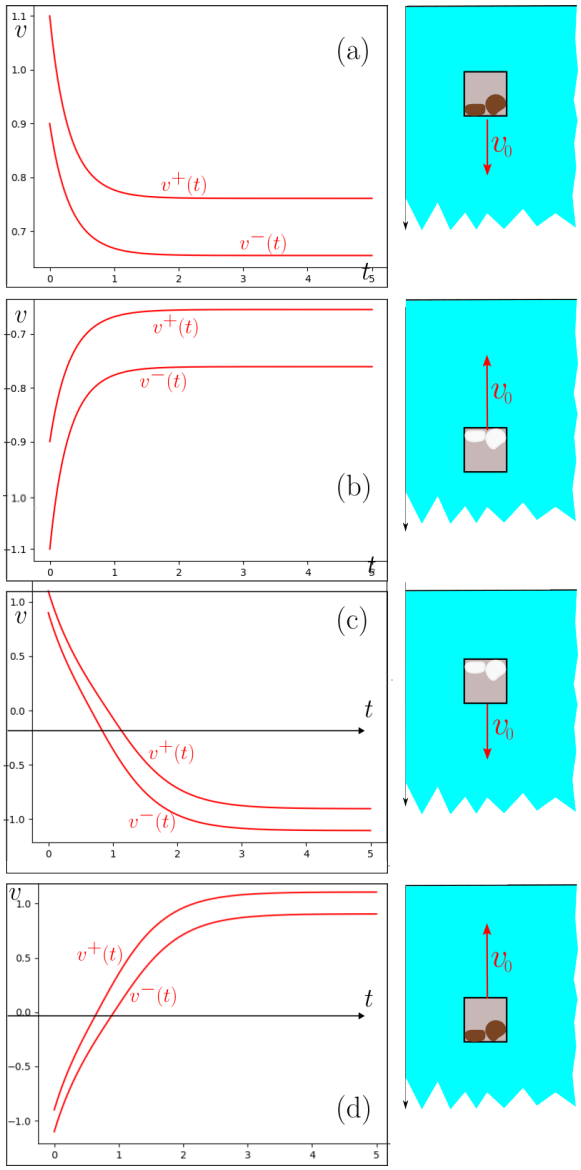


Figure 6: Sinking body (with stones inside) or floating body (with bubbles inside) for different initializations. There is no guarantee that the tubes contain the trajectory $v(t)$

3.3 Example: first order system

Consider a first order linear system with uncertain input u and initial state v:

$$\left\{ \begin{array}{c} \dot{v}(t) = av(t) + u(t) \\ v(0) = v_0 \in [v_0] \\ u(t) \in [\![u]\!] = [u^-, u^+] \end{array} \right. \tag{20}$$

From Proposition 2.1, we know that any solution $v(t)$ is inside $[v^-(t), v^+(t)]$, where:

$$\begin{array}{rcll} \dot{v}^- & = & av^- + u^- & , \quad v^-(0) = v_0^- \\ \dot{v}^+ & = & av^+ + u^+ & , \quad v^+(0) = v_0^+ \end{array} \tag{21}$$

i.e.

$$\begin{array}{rcl} v^-(t) & = & e^{at} v_0^- + \int_0^t e^{a(t-\tau)} u^-(\tau) d\tau \\ & = & e^{at} \left(v_0^- + \int_0^t e^{-a\tau} u^-(\tau) d\tau \right) \\ & = & e^{at} \left(v_0^- + u^- \int_0^t e^{-a\tau} d\tau \right) \\ & = & e^{at} \left(v_0^- + u^- \left[-\frac{1}{a} (e^{-a\tau}) \right]_0^t \right) \\ & = & e^{at} \left(v_0^- - \frac{u^-}{a} (e^{-at} - 1) \right) \\ v^+(t) & = & e^{at} \left(v_0^+ - \frac{u^+}{a} (e^{-at} - 1) \right) \end{array} \tag{22}$$

As a consequence, an interval flow for the scalar first order system is

$$\Phi_f(\delta, [v_0], [\![\mathbf{u}]\!]) = \left(\begin{array}{c} e^{a\delta} \left([v_0] - \frac{[\![u]\!]}{a} \left(e^{-a\delta} - 1 \right) \right) \\ e^{a[0,\delta]} \left([v_0] - \frac{[\![u]\!]}{a} \left(e^{-a[0,\delta]} - 1 \right) \right) \end{array} \right) \tag{23}$$

3.4 Real time interval integration

Recall that our goal is to integrate the equation of the float (1) with some interval uncertainties. Now, it will be shown later that the float is a serial composition of several subsystems for which we have an analytical interval flow. To show how this real-time interval integration can be done, we consider two compositions: serial and parallel, as illustrated by Figure 7. Note that the parallel composition will not we used for our application, but is given here to illustrate that our approach is not limited to serial systems.

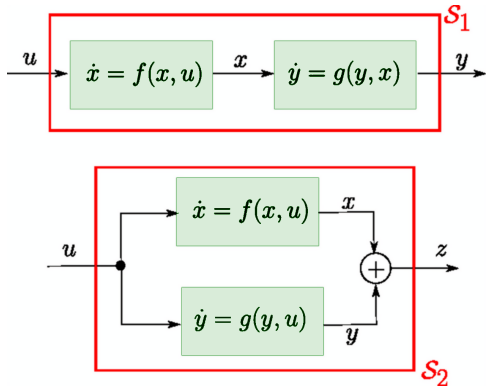


Figure 7: $\mathcal{S}_1$ is serial composition of two systems; $\mathcal{S}_2$ is a parallel composition

Serial systems Consider the system $\mathcal{S}_1$ (see Figure 7)

$$\mathcal{S}_1 : \left\{ \begin{array}{rcl} \dot{x} & = & f(x,u) \\ \dot{y} & = & g(y,x) \end{array} \right. \tag{24}$$

The following algorithm computes a tube for the output $y(t)$.

in: $[x_0], [y_0]$

1 $[x] = [x_0]$

2 $[y] = [y_0]$

3 for $k = 1$ to $k_{\max}$

4 Read $[\![u]\!] = [\![u]\!](k)$

5 $\begin{pmatrix} [x] \\ [\![x]\!] \end{pmatrix} = \Phi_f(\delta, [x], [\![u]\!])$

6 $\begin{pmatrix} [y] \\ [\![y]\!] \end{pmatrix} = \Phi_g(\delta, [y], [\![x]\!])$

7 write$(k, [y], [\![y]\!])$

Proof. Assume that,

$$\begin{array}{rcl} x(t_{k-1}) & \in & [x](k-1) \\ x([t_{k-1}-\delta, t_{k-1}]) & \in & [\![x]\!](k-1) \\ y(t_{k-1}) & \in & [y](k-1) \\ y([t_{k-1}-\delta, t_{k-1}]) & \in & [\![y]\!](k-1) \end{array} \tag{25}$$

with $t_k = k\delta$. Now, from Step 5,

$$\begin{pmatrix} [x](k) \\ [\![x]\!](k) \end{pmatrix} = \Phi_f(\delta, [x](k-1), [\![u]\!](k)) \tag{26}$$

From Equation (16),

$$\begin{cases} x(t_k) \in [x](k) \\ \forall t \in [t_k - \delta, t_k], x(t) \in [\![x]\!](k) \end{cases} \tag{27}$$

Moreover, from Step 6,

$$\begin{pmatrix} [y](k) \\ [\![y]\!](k) \end{pmatrix} = \Phi_f(\delta, [y](k-1), [\![x]\!](k)) \tag{28}$$

Thus, from (16),

$$\begin{cases} y(t_k) \in [y](k) \\ \forall t \in [t_k - \delta, t_k], y(t) \in [\![y]\!](k) \end{cases} \tag{29}$$

□

Parallel systems Consider the system $\mathcal{S}_2$ of Figure 7:

$$\mathcal{S}_2 : \begin{cases} \dot{x} &= f(x,u) \\ \dot{y} &= g(y,u) \\ z &= x+y \end{cases} \tag{30}$$

The following algorithm computes a tube for the output $z(t)$.

in: $[x_0], [y_0]$

1 $[x] = [x_0]$

2 $[y] = [y_0]$

3 for $k = 1$ to $k_{\max}$

4 Read $[\![u]\!] = [\![u]\!](k)$

5 $\begin{pmatrix} [x] \\ [\![x]\!] \end{pmatrix} = \Phi_f(\delta, [x], [\![u]\!])$

6 $\begin{pmatrix} [y] \\ [\![y]\!] \end{pmatrix} = \Phi_g(\delta, [y], [\![u]\!])$

7 $\begin{pmatrix} [z] \\ [\![z]\!] \end{pmatrix} = \begin{pmatrix} [x]+[y] \\ [\![y]\!]+[\![y]\!] \end{pmatrix}$

8 write$(k, [z], [\![z]\!])$

Proof. The proof is similar to that provided for serial systems. □

4 Analytical solution of the Riccati equation

To be able to simulate our float with an interval uncertainty, we need to find an interval flow for each of the three blocks of Figure 4. For the first and the last blocks which are both integrators, the interval flow has been given in Subsection 3.2. For the block of the middle, the interval flow needs a specific analytical resolution. Now, this resolution can be derived from the analytical solution of a Riccati equation that is considered in this section. All results given here are taken from [19] but only those that are useful for our application have been extracted from this book.

A Riccati equation is given by

$$\dot{v} = a - bv^2. \tag{31}$$

We assume here that $v_0 > 0$.

Proposition. *If $a > 0$ then the solution of (31) is*

$$\begin{array}{rcl} v(t) & = & \bar{v}\frac{ce^{2\sqrt{ab}t}-1}{ce^{2\sqrt{ab}t}+1} \\ c & = & \frac{\bar{v}+v_0}{\bar{v}-v_0} \\ \bar{v} & = & \sqrt{\frac{a}{b}} \end{array} \tag{32}$$

Proof. Set $E(t) = ce^{2\sqrt{ab}t}$, we have $\dot{E} = 2\sqrt{ab}cE$. We have

$$\begin{array}{rl} & \dot{v} = a - bv^2 \\ \Leftrightarrow & \bar{v}\frac{d}{dt}\left(\frac{E-1}{E+1}\right) = a - b\left(\bar{v}\frac{E-1}{E+1}\right)^2 \\ \Leftrightarrow & \bar{v}\left(\frac{\dot{E}(E+1)-\dot{E}(E-1)}{(E+1)^2}\right) = a - b\left(\bar{v}\frac{E-1}{E+1}\right)^2 \\ \Leftrightarrow & \bar{v}\left(\frac{2\sqrt{ab}cE(E+1)-2\sqrt{ab}cE(E-1)}{(E+1)^2}\right) = a - b\left(\bar{v}\frac{E-1}{E+1}\right)^2 \\ \Leftrightarrow & \sqrt{\frac{a}{b}}\left(2\sqrt{ab}E\,(E+1) - 2\sqrt{ab}E\,(E-1)\right) = a\,(E+1)^2 - a\,(E-1)^2 \\ \Leftrightarrow & 4aE = E^2 + 2aE + 1 - \left(E^2 + 2aE + 1\right) \end{array} \tag{33}$$

which is true. □

The solution of the Riccati equation, as given by Proposition 4 is singular when $a = 0$ and numerically ill-conditioned a is near zero. Now, this singularity has no physical reason and can be avoided by the using the *exponential cardinal* function expc(ν) defined by

$$\mathrm{expc}(\nu) = \frac{e^{\nu} - 1}{\nu} \tag{34}$$

with expc(0) = 1. This function is continuous and differentiable everywhere. It is a monotonic function, strictly positive and its graph is similar to that of $\exp \nu$. The singularity we observe in the expression for $\nu = 0$ is artificial and should not be considered as such.

Proposition. *If $a \geq 0$ then the solution of (31) is*

$$v(t) = \frac{e^{2b\bar{v}t}(\bar{v}+v_0)+v_0-\bar{v}}{1+e^{2b\bar{v}t}+2v_0bt\cdot \mathrm{expc}(2b\bar{v}t)} \tag{35}$$

Note that, thanks to the use of the expc function, this expression for $v(t)$ has no more singularity for $t=0$.

Proof. Let us first check that the formula is correct when $a>0$. We have

$$\begin{array}{rcccl} v(t) & = & \bar{v}\frac{\frac{\bar{v}+v_0}{\bar{v}-v_0}e^{2b\bar{v}t}-1}{\frac{\bar{v}+v_0}{\bar{v}-v_0}e^{2b\bar{v}t}+1} & = & \bar{v}\frac{(\bar{v}+v_0)e^{2b\bar{v}t}-(\bar{v}-v_0)}{(\bar{v}+v_0)e^{2b\bar{v}t}+(\bar{v}-v_0)} \\ & = & \bar{v}\frac{\bar{v}\left(e^{2b\bar{v}t}-1\right)+v_0\left(e^{2b\bar{v}t}+1\right)}{\bar{v}\left(e^{2b\bar{v}t}+1\right)+v_0\left(e^{2b\bar{v}t}-1\right)} & = & \frac{\bar{v}\left(e^{2b\bar{v}t}-1\right)+v_0\left(e^{2b\bar{v}t}+1\right)}{\left(e^{2b\bar{v}t}+1\right)+v_0\left(\frac{e^{2b\bar{v}t}-1}{\bar{v}}\right)} \\ & = & \frac{\bar{v}\left(e^{2b\bar{v}t}-1\right)+v_0\left(e^{2b\bar{v}t}+1\right)}{\left(e^{2b\bar{v}t}+1\right)+2v_0bt\cdot\mathrm{expc}(2b\bar{v}t)} & & \end{array} \tag{36}$$

Let is now check that the formula is correct when $a=0$. Since $\bar{v}=\sqrt{\frac{a}{b}}=0$, we have

$$v(t) = \frac{v_0\left(e^0+1\right)}{1+e^0+2v_0bt} = \frac{v_0}{1+v_0bt}. \tag{37}$$

Thus

$$\begin{array}{rcc} & \dot{v}=a-bv^2 & \\ \Leftrightarrow & \dot{v}=-bv^2 & \\ \Leftrightarrow & v_0\frac{-v_0b}{(1+v_0bt)^2} = -b\left(\frac{v_0}{1+v_0bt}\right)^2 & \end{array} \tag{38}$$

which is true. □

Proposition. *If $a<0$ then the solution of (31) is*

$$\begin{array}{rcl} v(t) & = & \bar{v}\tan\left(\mathrm{atan}\,\frac{v_0}{\bar{v}}-b\bar{v}t\right) \\ \bar{v} & = & -\sqrt{\frac{-a}{b}} \end{array} \tag{39}$$

where

$$t<t_1=\frac{1}{-b\bar{v}}\left(\frac{\pi}{2}-\mathrm{atan}\,\frac{v_0}{\bar{v}}\right). \tag{40}$$

The change of sign for $v(t)$ is obtained for

$$t_2=\frac{1}{b\bar{v}}\,\mathrm{atan}\,\frac{v_0}{\bar{v}}. \tag{41}$$

Proof. First, note that $a=-\bar{v}^2b$. We have

$$\begin{array}{rcc} & \dot{v}=a-bv^2 & \\ \Leftrightarrow & \frac{d}{dt}\left(\bar{v}\tan\left(\mathrm{atan}\,\frac{v_0}{\bar{v}}-b\bar{v}t\right)\right) = -\bar{v}^2b-b\bar{v}^2\tan^2\left(\mathrm{atan}\,\frac{v_0}{\bar{v}}-b\bar{v}t\right) & \\ \Leftrightarrow & \left(1+\tan^2\left(\mathrm{atan}\,\frac{v_0}{\bar{v}}-b\bar{v}t\right)\right)\cdot\underbrace{\frac{d}{dt}\left(\mathrm{atan}\,\frac{v_0}{\bar{v}}-b\bar{v}t\right)}_{-b\bar{v}} = -\bar{v}b\left(1+\tan^2\left(\mathrm{atan}\,\frac{v_0}{\bar{v}}-b\bar{v}t\right)\right) & \\ \Leftrightarrow & 1+\left(\tan\left(\mathrm{atan}\,\frac{v_0}{\bar{v}}-b\bar{v}t\right)\right)^2 = 1+\left(\tan\left(\mathrm{atan}\,\frac{v_0}{\bar{v}}-b\bar{v}t\right)\right)^2 & \end{array}$$

which is true. The integration is possible until

$$\operatorname{atan}\frac{v_0}{\bar{v}} - b\bar{v}t \in \left]-\frac{\pi}{2}, \frac{\pi}{2}\right[\tag{42}$$

This condition is satisfied for $t = 0$. It will still be satisfied until

$$\begin{array}{rl} & \operatorname{atan}\frac{v_0}{\bar{v}} - b\bar{v}t \leq \frac{\pi}{2} \\ \Leftrightarrow \qquad & t \leq t_1 = \frac{1}{-b\bar{v}}\left(\frac{\pi}{2} - \operatorname{atan}\frac{v_0}{\bar{v}}\right) \end{array} \tag{43}$$

For this t_1, the solution is at infinity. For the initialization, we need to have $\operatorname{atan}\frac{v_0}{\bar{v}} \in]-\frac{\pi}{2}, \frac{\pi}{2}[$ which is always the case. To get the time of change of sign for $v(t)$, we solve:

$$\operatorname{atan}\frac{v_0}{\bar{v}} - b\bar{v}t_2 = 0. \tag{44}$$

Thus

$$t_2 = \frac{1}{b\bar{v}}\operatorname{atan}\frac{v_0}{\bar{v}}. \tag{45}$$

□

Corollary. *The solution of the Riccati equation* $\dot{v} = a - bv^2$ *for* $b > 0$ *is*

$$\begin{array}{rcccl} v(t) & = & \psi^+_{a,b,v_0}(t) & = & \frac{e^{2b\bar{v}t}(\bar{v}+v_0)+v_0-\bar{v}}{1+e^{2b\bar{v}t}+2v_0bt\,\mathrm{expc}(2b\bar{v}t)} \qquad \text{if } a \geq 0 \\ & = & \psi^-_{a,b,v_0}(t) & = & \bar{v}\tan\left(\operatorname{atan}\frac{v_0}{\bar{v}} - b\bar{v}t\right) \qquad \text{if } a < 0 \end{array} \tag{46}$$

where $\bar{v} = \operatorname{sign}(a)\sqrt{\frac{|a|}{b}}$.

5 Sinking body problem

We consider again the equation of the sinking body given by

$$\dot{v} = a - bv|v| \tag{47}$$

where $b > 0$. This equation is close to the Riccati equation $\dot{v} = a - bv^2$. Equivalently (47) can be seen as a piecewise Riccati equation. In this section, we propose to find an analytic solution for the solution $v(t)$. This expression is needed to build an interval flow for (47) which will then be used to integrate our float with interval uncertainties.

5.1 Analytical expression of the solution of the sinking body motion

From the analytical solution of the Riccati equation, we can get an analytical expression of the sinking body motion in the case where the parameters a, b are constant.

Proposition. *The solution of* $\dot{v} = a - bv|v|$ *is*

$$\varphi_{a,b,v_0}(t) = \begin{cases} \operatorname{sign}(a) \cdot \psi^+_{|a|,b,\operatorname{sign}(a)\cdot v_0}(t) & \text{if } av_0 \geq 0 \\ -\operatorname{sign}(a) \cdot \psi^-_{-|a|,b,-\operatorname{sign}(a)\cdot v_0}(t) & \text{if } av_0 < 0 \text{ and } t \leq t_2 \\ \operatorname{sign}(a) \cdot \psi^+_{|a|,b,0}(t - t_2) & \text{if } av_0 < 0 \text{ and } t > t_2 \end{cases} \tag{48}$$

where $t_2 = -\frac{\operatorname{sign}(a)}{\sqrt{|a|b}} \operatorname{atan}\left(v_0\sqrt{\frac{b}{|a|}}\right)$, *where* ψ^- *and* ψ^+ *are defined by (46).*

Proof. If $a = 0$ or $v_0 = 0$, we have $av_0 \geq 0$ and we easily check that the Proposition is valid. We need to check four cases.

Case 1 $a > 0, v_0 > 0$. We have $\dot{v} = a - bv^2$ which is a Riccati equation. From Corollary 4, $v(t) = \psi^+_{a,b,v_0}(t)$ for all $t \geq 0$.

Case 2 $a < 0, v_0 < 0$. We have $\dot{v} = a - bv|v| = a + bv^2$. Set $w = -v$. We have $-\dot{w} = a + bw^2$, *i.e.*, $\dot{w} = (-a) - bw^2$. Thus $w(t) = \psi^+_{-a,b,w_0}(t)$ and finally

$$v(t) = -\psi^+_{-a,b,-v_0}. \tag{49}$$

Case 3 $a < 0, v_0 > 0$. We have $\dot{v} = a - bv^2$, which is again a Riccati equation. From Corollary 4, we get

$$\begin{array}{rcll} v(t) & = & \psi^-_{a,b,v_0}(t) & \text{if } t \leq t_2 = \frac{1}{b\bar{v}} \operatorname{atan} \frac{v_0}{\bar{v}} \\ v(t) & = & -\psi^+_{-a,b,0}(t - t_2) & \text{if } t > t_2 \end{array} \tag{50}$$

Case 4 $a > 0, v_0 < 0$. We have $\dot{v} = a - bv|v| = a + bv^2$. We get

$$\begin{array}{rcll} v(t) & = & -\psi^-_{-a,b,-v_0}(t) & \text{if } t \leq t_2 = -\frac{1}{b\bar{v}} \operatorname{atan} \frac{v_0}{\bar{v}} \\ v(t) & = & \psi^+_{a,b,0}(t - t_2) & \text{if } t > t_2 \end{array} \tag{51}$$

□

5.2 Interval flow of the sinking body motion

Corollary. *If* $v_0 \in [v_0^-, v_0^+]$, $a \in [a^-, a^+], b \in [b^-, b^+]$ *and* $t \in [t^-, t^+]$, *we have*

$$\varphi_{a,b,v_0}(t) \in [\varphi]_{[a],[b],[v_0]}([t]) \tag{52}$$

where

$$(i) \quad [\varphi]_{[a],[b],[v_0]}([t])) = [\varphi]_{a^-,[b],v_0^-}([t]) \sqcup [\varphi]_{a^+,[b],v_0^+}([t]) \tag{53}$$

$$(ii) \quad [\varphi]_{a,[b],v_0}([t]) = [\varphi]_{a,[b],v_0}(\{t^-, t^+\}) \tag{54}$$

$$(iii) \quad [\varphi]_{a,[b],v_0}(t) = \begin{cases} \sigma \cdot [\psi^+]_{|a|,[b],\sigma v_0}(t) & \text{if } a \cdot v_0 \geq 0 \\ [\hat{\varphi}]_{a,[b],v_0}(t) & \text{if } a \cdot v_0 < 0 \end{cases} \tag{55}$$

$$(iv) \quad [\hat{\varphi}]_{a,[b],v_0}(t) = \begin{cases} \varphi_{a,\{b^-,b^+\},v_0}(t)) & \text{if } t \notin [t_2] \\ \sigma \cdot [\psi^+]_{|a|,[b],0}(t - [t_2]) & \text{if } t \in [t_2] \\ [t_2] = t_2(v_0, a, \{b^-, b^+\}) \end{cases} \tag{56}$$

$$(v) \quad [\psi^+]_{a,[b],v_0}(t) = \psi^+_{a,\{b^-,b^+\},v_0}(t) \tag{57}$$

where

$$\begin{array}{rcl} t_2(v_0, a, b) & = & -\frac{\sigma}{\sqrt{|a| \cdot b}} \operatorname{atan}\left(v_0 \sqrt{\frac{b}{|a|}}\right) \\ \sigma & = & \operatorname{sign}(a) \end{array}$$

and $\sqcup$ *denotes the interval hull operator.*

Remark. In the previous formulas, we use an enumeration notation with braces. The resulting calculus returns the smallest interval which contains all possibilities obtained from the list. For instance

$$\begin{array}{rcll} \sin(\{0,1\}) & = & [0, \sin(1)] & \\ [\varphi]_{a,[b],v_0}(\{t^-, t^+\}) & = & [\varphi]_{a,[b],v_0}(t^-) \sqcup [\psi]_{a,[b],v_0}(t^+) & \text{(see Corollary 5.2, (ii))} \\ \psi^+_{a,\{b^-,b^+\},v_0}(t) & = & \left[\left\{\psi^+_{a,b^-,v_0}(t), \psi^+_{a,b^+,v_0}(t)\right\}\right] & \text{(see Corollary 5.2, (v))} \end{array}$$

Proof. (i) Using the comparison theorem, we have

$$v_0 \in [v_0^-, v_0^+], a \in [a^-, a^+] \Rightarrow \varphi_{a,b,v_0}(t) \in \left[\varphi_{a^-,b,v_0^-}(t), \varphi_{a^+,b,v_0^+}(t)\right].$$

It suffices to enclose the two quantities $\psi_{a^-,b,v_0^-}(t)$ and $\psi_{a^+,b,v_0^+}(t)$.

(ii) The signal $\dot{v}(t)$ can never change of sign. Indeed, $\dot{v}(t) = 0$ if $a - bv|v| = 0$ and in this case, $\dot{v}(t) = 0$ for all t. As a consequence, the extreme values for $\varphi_{a,b,v_0}(t)$ are obtained for $t \in \{t^-, t^+\}$.

(iii) Assume that (a, v_0, t) is fixed. If $a \cdot v_0 \geq 0$, we have no stop point. Thus $\varphi_{a,b,v_0}(t) = \sigma \cdot {\psi^+}_{|a|,[b],\sigma v_0}(t)$ as seen in 48. Otherwise, we are in a situation with a stop point.

(iv) We have a stop point. This stop point can be inside or outside the time window $[t]$. We have

$$\frac{\partial \varphi_{a,b,v_0}(t)}{\partial b} = 0 \Leftrightarrow t = t_2 = -\frac{\operatorname{sign}(a)}{\sqrt{|a|b}} \operatorname{atan}\left(v_0 \sqrt{\frac{b}{|a|}}\right). \tag{58}$$

Thus, if $t \notin [t_2]$, where $[t_2] = t_2(v_0, a, \{b^-, b^+\})$, $\varphi_{a,b,v_0}(t)$ is monotonic in t and thus

$$\varphi_{a,b,v_0}(t) \in \varphi_{a,\{b^-,b^+\},v_0}(t) \tag{59}$$

otherwise

$$\varphi_{a,b,v_0}(t) \in \sigma \cdot {\psi^+}_{|a|,[b],0}(t - t_2(v_0, a, \{b^-, b^+\})). \tag{60}$$

(v) The result comes from the monotonicity of ψ^+ with respect to b. □

Corollary. *An interval flow of the sinking body motion is:*

$$\Phi_f : \begin{array}{ccc} \mathbb{IR} \times \mathbb{IR}^2 & \to & \mathbb{IR} \times \mathbb{IR} \\ ([v_0], [\![a]\!], [\![b]\!]) & \to & \begin{pmatrix} [v] \\ [\![v]\!] \end{pmatrix} = \begin{pmatrix} [\varphi]_{[\![a]\!],[\![b]\!],[v_0]}(\delta) \\ [\varphi]_{[\![a]\!],[\![b]\!],[v_0]}([0,\delta]) \end{pmatrix} \end{array} \tag{61}$$

5.3 Example

We take again four cases already treated in Subsection 2.2 (Figure 8).

Case a We have $(v_0, a, b) \in [0.9, 1.1] \times [0.9, 1.1] \times [1.9, 2.1]$. In red, we have the envelope already obtained by the Runge-Kutta method. No pessimism can be observed which is consistent with the fact that $\varphi_{a,b,v_0}(t)$ is monotonic. The magenta bar corresponds to the initial interval $[0.9, 1.1]$ for v_0.

Case b We have $(v_0, a, b) \in [-1.1, -0.9] \times [-1.1, -0.9] \times [1.9, 2.1]$. The envelope is symmetrical to that obtained for Case a. Again, due to the monotonicity $\varphi_{a,b,v_0}(t)$, no pessimism can be observed.

Case c We have $(v_0, a, b) \in [0.9, 1.1] \times [-1.1, -0.9] \times [1.9, 2.1]$. The pessimism of the enclosure is too small to be observed; compared to the trajectories obtained by a Runge Kutta integration (red). From the tube, we can conclude that the speed of the float will cancel and the float will come back.

Case d We have $(v_0, a, b) \in [-1.1, -0.9] \times [0.9, 1.1] \times [1.9, 2.1]$. The situation is similar to that given in Case c.

In the figures, the units are t(sec) and v (m/sec).

6 Online integration of the float

Consider again the float described by Equation (1). Due to the serial structure of the system, we can integrate the differential inclusion using interval flows for each component, as explained in Subsection 3.4. The corresponding decomposition is expressed by Figure 9 and is consistent with the initial goal (see Equation 5). For each sampling time, five steps have to be performed sequentially in the right order. Between sampling times k to $k+1$, three intervals have to be transmitted through the memory: $[s](k), [v](k), [d](k)$.

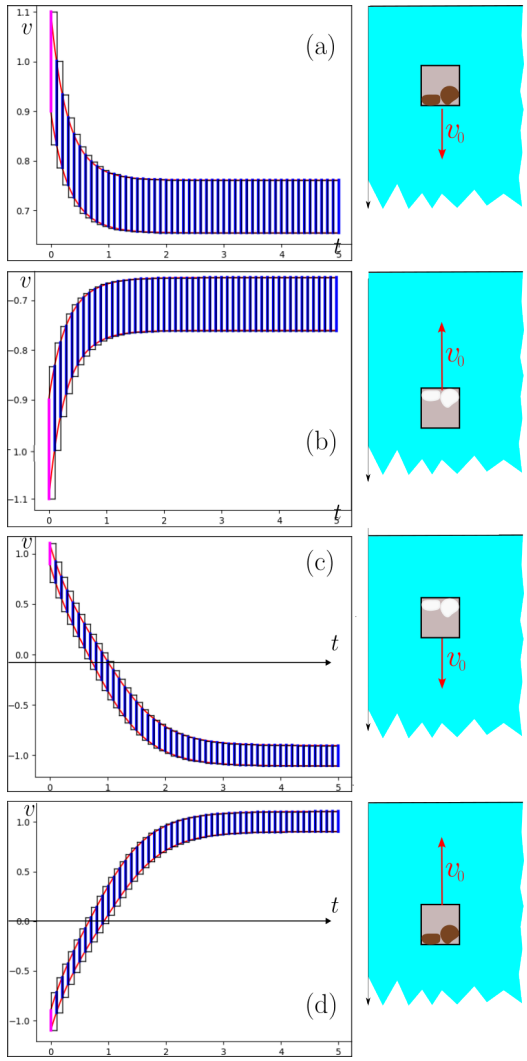


Figure 8: Sinking body for four different initializations. The tubes contains the trajectory $v(t)$

At Step 1, we read the input slice $[\![u]\!](k)$ which contains all $u(t)$ for $t \in [(k-1)\delta, k\delta]$. At Step 2, we integrate $[\![u]\!]$ using the interval flow for the integrator presented in Subsection 3.2. As a result, we get a slice $[\![s]\!](k)$ for $s(t)$. Using a static interval evaluation, we then get at Step 3 two slices $[\![a]\!](k)$ for $a(t)$ and $[\![b]\!](k)$ for $b(t)$. These two slices will then feed the interval flow $[\varphi]_{[\![a]\!],[\![b]\!],[v]}$ which yields the slice $[\![v]\!](k)$ and the gate $[v](k)$ at Step 4. The slice $[\![v]\!](k)$ is then used at Step 5 by the last block to generate the slice $[\![d]\!](k)$ and the gate $[d](k)$.

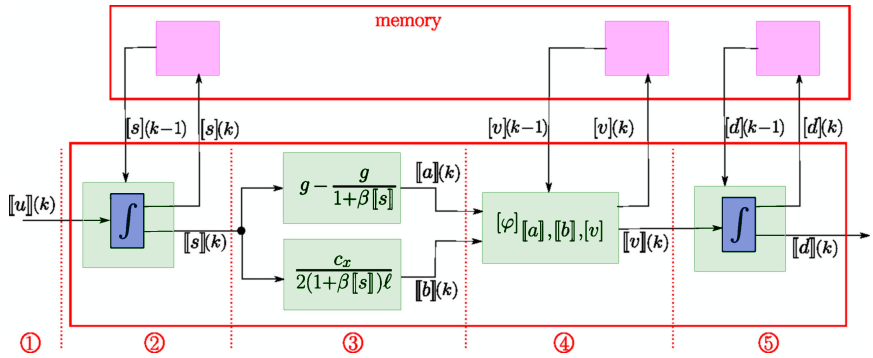


Figure 9: Sequence to be followed for one step interval integration

The resulting computations correspond to the following algorithm.

$$
\begin{array}{ll}
\text{In:} & [d_0], [v_0], [s_0] \\
\text{Init} & [d] = [d_0] \\
& [v] = [v_0] \\
& [s] = [s_0]
\end{array}
$$

$$
\begin{array}{ll}
\text{Main loop} & \text{For } k = 1 \text{ to } k_{\max} \\
\text{Step 1} & \text{Read } [\![u]\!] = [\![u]\!](k) \\
\text{Step 2} & [\![s]\!] = [s] + [\![u]\!] \cdot [0, \delta] \\
& [s] = [s] + [\![u]\!] \cdot \delta \\
\text{Step 3} & [\![a]\!] = g \cdot \left(1 - \frac{1}{1+\beta[\![s]\!]}\right) \\
& [\![b]\!] = \frac{c_x}{2(1+\beta[\![s]\!])\ell} \\
\text{Step 4} & [\![v]\!] = [\varphi]_{[\![a]\!],[\![b]\!],[v]}([0, \delta]) \\
& [v] = [\varphi]_{[\![a]\!],[\![b]\!],[v]}(\delta) \\
\text{Step 5} & [\![d]\!] = [d] + [\![v]\!] \cdot [0, \delta] \\
& [d] = [d] + [\![v]\!] \cdot \delta \\
& \text{write}(k, [d], [\![d]\!], [v], [\![v]\!], [s], [\![s]\!])
\end{array}
$$

The only memory needed by this interval simulator are the three gates $[s], [v], [d]$.

The behavior of the interval simulator is illustrated by Figure 10. We took $g_0 = 9.81m \cdot s^{-2}, \ell = 1m, \beta = 0.1, c_x = 0.9$ for the parameters and $[s_0] = [v_0] = [d_0] = [0, 0.1]$ for the initial conditions. For the input, we took $[\![u]\!](k) = \exp(-[(k-1)\delta, k\delta])$. In the figures, the chosen units are t(sec), d(m) and v (m/sec).

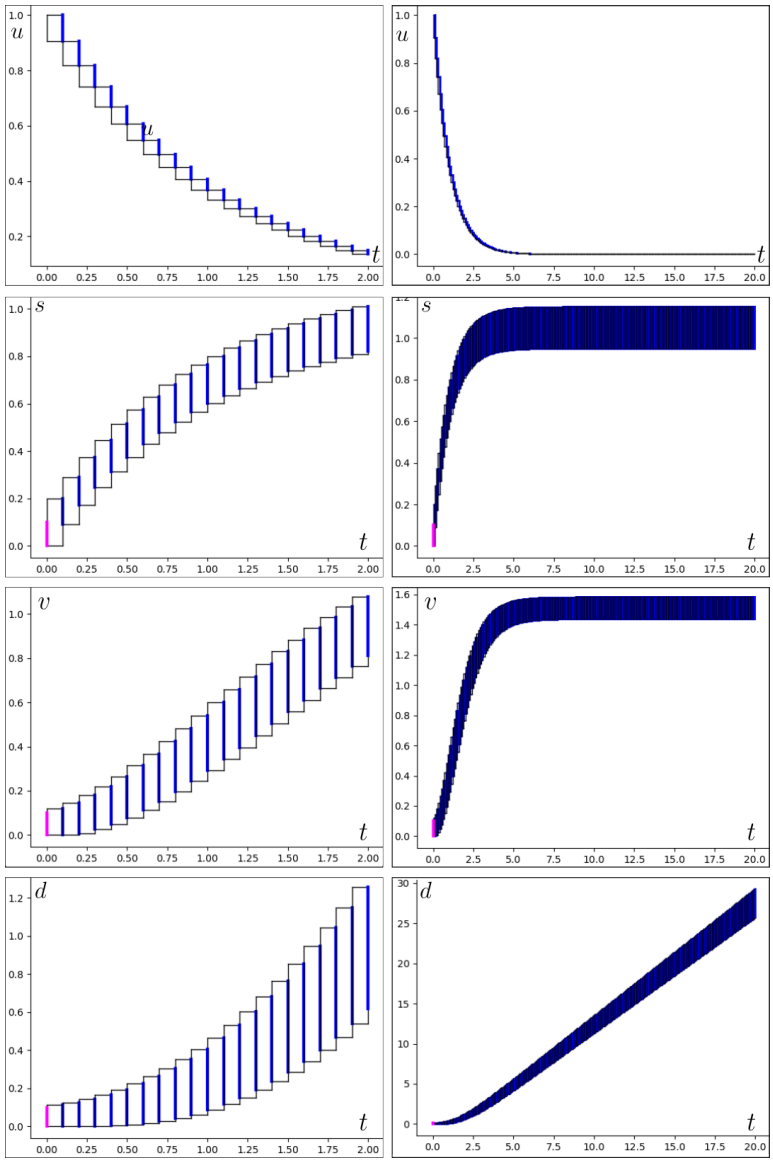


Figure 10: Sinking float. The tubes contain the trajectories $u(t), s(t), v(t), d(t)$ for $t \in [0, 2]$ (left) and for $t \in [0, 20]$ (right)

Even if the system is unstable in the Lyapunov sense (indeed the variable d tends to infinity), we do not observe any exponential explosion of the pessimism, unlike other existing interval methods dealing with differential inclusions.

The implementation is done using the Codac library [23] and the source codes are available at https://www.ensta-bretagne.fr/jaulin/reachfloat.html.

7 Conclusion

In this paper, a new interval estimator has been proposed for online state prediction. For this, we have introduced the concept of interval flow that has to be found analytically for each component of the whole system. Combining the interval flows of all subsystems, we have shown that an interval estimator containing the state variables in a guaranteed way could be derived. For simplicity, but also to evaluate the accuracy of the approach, only the reachability problem has been addressed. This means that no exteroceptive measurements (*i.e.*, collected by a sensor able to interact with the environment, such as a camera, a lidar or a radar) have been taken into account in order to contract the domains for the state variables. The interval state estimator that has been obtained has a fixed number of operations to be performed at each sampling time. This is a strong requirement rarely considered by classical interval algorithms. Indeed, existing interval algorithms dealing with differential inclusions use fixed point procedures that are not consistent with real-time issues. Through an example taken from robotics (an underwater robot with a ballast), we have shown that it was possible to deal with engineering systems efficiently.

The presented approach can be applied to a complex system as soon as it can be built using a parallel and a serial composition of specific scalar systems [12]. More precisely, these scalar systems should have a single state variable, may have several inputs, and an analytical solution should be available for constant inputs. The existence of such an analytical solution could be relaxed if we accept to use an interval resolution of a differential equation based on the Picard operator [13].

References

[1] Alamo, T., Bravo, J., and Camachoa, E. Guaranteed state estimation by zonotopes. *Automatica*, 41(6):1035–1043, 2005. DOI: 10.1016/j.automatica.2004.12.008.

[2] Alexandre dit Sandretto, J. and Chapoutot, A. Validated simulation of differential algebraic equations with Runge-Kutta methods. *Reliable Computing*, 22:56–77, 2016. DOI: 10.1007/s11155-016-0001-2.

[3] Althoff, M. and Krogh, B. Zonotope bundles for the efficient computation of reachable sets. In *Proceedings of the 2011 50th IEEE Conference on Decision and Control and European Control Conference*, pages 6814–6821, 2011. DOI: 10.1109/CDC.2011.6160872.

[4] Asarin, E., Dang, T., and Girard, A. Reachability analysis of nonlinear systems using conservative approximation. In Maler, O. and Pnueli, A., editors, *Hybrid*

Systems: Computation and Control, Volume 2623 of *Lecture Notes in Computer Science*, pages 20–35. Springer, 2003. DOI: 10.1007/3-540-36580-X_5.

[5] Aubin, J. and Frankowska, H. *Set-Valued Analysis*. Birkhäuser, Boston, Boston, MA, 1990. DOI: 10.1007/978-0-8176-4848-0.

[6] Collins, P. and Goldsztejn, A. The reach-and-evolve algorithm for reachability analysis of nonlinear dynamical systems. *Electronic Notes in Theoretical Computer Science*, 223:87–102, 2008. DOI: 10.1016/j.entcs.2008.12.033.

[7] Combastel, C. A state bounding observer for uncertain non-linear continuous-time systems based on zonotopes. In *Proceedings of the 44th IEEE Conference on Decision and Control*, pages 7228–7234. IEEE, 2005. DOI: 10.1109/CDC.2005.1583327.

[8] Efimov, D. and Raïssi, T. Design of interval observers for uncertain dynamical systems. *Automation and Remote Control*, 77(2):191–225, 2016. DOI: 10.1134/S0005117916020016.

[9] Frehse, G. PHAVer: Algorithmic verification of hybrid systems past HyTech. *International Journal on Software Tools for Technology Transfer*, 10:263–279, 2008. DOI: 10.1007/s10009-007-0062-x.

[10] Goubault, E., Mullier, O., Putot, S., and Kieffer, M. Inner approximated reachability analysis. In *Proceedings of the 17th International Conference on Hybrid Systems: Computation and Control*, pages 163–172. ACM, 2014. DOI: 10.1145/2562059.2562113.

[11] Guernic, C. L. and Girard, A. Reachability analysis of linear systems using support functions. *Nonlinear Analysis: Hybrid Systems*, 4(2):250–262, 2010. DOI: 10.1016/j.nahs.2009.03.003.

[12] Jaulin, L. Integral algebra for simulating dynamical systems with interval uncertainties. *International Journal of Approximate Reasoning*, 178, 2025. DOI: doi.org/10.1016/j.ijar.2024.109353.

[13] Kapela, T., Mrozek, M., Wilczak, D., and Zgliczynski, P. CAPD: DynSys, A flexible C++ toolbox for rigorous numerical analysis of dynamical systems. *Communications in Nonlinear Science and Numerical Simulation*, 101:105578, 2021. DOI: 10.1016/j.cnsns.2020.105578.

[14] Kieffer, M., Jaulin, L., and Walter, E. Guaranteed recursive nonlinear state estimation using interval analysis. In *Proceedings of the 37th IEEE Conference on Decision and Control*, pages 3966–3971, Tampa, FL, USA, 1998. IEEE. DOI: 10.1109/CDC.1998.761926.

[15] LaValle, S. *Planning Algorithm*. Cambridge University Press, 2006. DOI: 10.1017/CBO9780511546877.

[16] Mitchell, I., Bayen, A., and Tomlin, C. Validating a Hamilton-Jacobi approximation to hybrid system reachable sets. In Benedetto, M. and Sangiovanni-Vincentelli, A., editors, *Hybrid Systems: Computation and Control*, Volume 2034 of *Lecture Notes in Computer Science*, pages 418–432. Springer Berlin Heidelberg, 2001. DOI: 10.1007/3-540-45351-2_34.

[17] Moore, R. *Methods and Applications of Interval Analysis*. Society for Industrial and Applied Mathematics, 1979. DOI: 10.1137/1.9781611970906.

[18] Munson, B., Young, D., Okiishi, T., and Huebsch, W. *Fundamentals of Fluid Mechanics*. John Wiley & Sons, 7th edition, 2013. DOI: 10.1002/9781118912652.

[19] Polyanin, A., Andrei, D., and Zaitsev, V. *Handbook of Exact Solutions for Ordinary Differential Equations*. Chapman and Hall, CRC, 2nd edition, 2003. DOI: 10.1201/9781420035330.

[20] Ramdani, N. and Nedialkov, N. Computing reachable sets for uncertain nonlinear hybrid systems using interval constraint-propagation techniques. *Nonlinear Analysis: Hybrid Systems*, 5(2):149–162, 2011. DOI: 10.1016/j.nahs.2010.05.010.

[21] Rauh, A., Kersten, J., and Aschemann, H. Techniques for verified reachability analysis of quasi-linear continuous-time systems. In *Proceedings of the 2019 24th International Conference on Methods and Models in Automation and Robotics*, pages 18–23, 2019. DOI: 10.1109/MMAR.2019.8864648.

[22] Rauh, A., Lahme, M., Rohou, S., Jaulin, L., Dinh, T., Raïssi, T., and Fnadi, M. Offline and online use of interval and set-based approaches for control and state estimation: A review of methodological approaches and their application. *Logical Methods in Computer Science*, 2023. DOI: 10.48550/arXiv.2309.11622.

[23] Rohou, S., Desrochers, B., and Bars, F. L. The codac library. *Acta Cybernetica*, 26(4):871–887, 2024. DOI: 10.14232/ACTACYB.302772.

[24] Rohou, S., Jaulin, L., Mihaylova, L., Bars, F. L., and Veres, S. *Reliable Robot Localization*. Wiley, 2019. DOI: 10.1002/9781119680970.

[25] Smith, H. Monotone dynamical systems: An introduction to the theory of competitive and cooperative systems. *Mathematical Surveys and Monographs*, 41, 1995. DOI: 10.1090/surv/041.

[26] Taha, W. and Duracz, A. Acumen: An open-source testbed for cyber-physical systems research. In *Conference on CYber physiCaL systems, iOt and sensors Networks*, 2015. DOI: 10.1007/978-3-319-47063-4_11.

[27] Wan, J. *Computationally reliable approaches of contractive model predictive control for discrete-time systems*. PhD dissertation, Universitat de Girona, Girona, Spain, 2007. URL: http://www.tdx.cat/TDX-1008107-141828.